Proceedings of ASME Turbo Expo 2011: Power for Land, Sea and Air
GT2011
June 6-10, 2011, Vancouver, Canada

DRAFT

GT2011-46182

THE EFFECT OF THE CASING MOVEMENT RELATIVE TO THE BLADES ON THE TIP LEAKAGE LOSS IN AXIAL FLOW COMPRESSORS

Guillaume PALLOT, Dai KATO, Hidekazu KODAMA
IHI Corporation
Mizuho, Tokyo, Japan

Kazunari MATSUDA, Hideo TANIGUCHI, Hiromasa KATO, Ken-ichi FUNAZAKI
Iwate University
Morioka, Iwate, Japan

ABSTRACT

This paper investigates the effect of the casing movement relative to the blades on the tip leakage loss generation mechanisms by using experimental results from a linear cascade test facility, and viscous numerical results. Traverse measurements in the pitch-wise and span-wise directions are made using a five-hole Pitot tube at the inlet and exit planes of a compressor linear cascade comprising seven equally-pitched blades. The blades are two-dimensionally stacked with a cross section representing a typical rear stage rotor of a highly loaded axial-flow compressor. A moving belt, driven by a motor and a pulley system, runs linearly at constant speed under the horizontally suspended cascade to simulate the relative motion of the blade and the casing. Tip clearance can be adjusted by changing the height of the blades. The experimental results, at 2% and 4% tip clearance to blade heights, indicate that the tip leakage loss decreases when the casing is in movement. The Reynolds-averaged Navier-Stokes numerical calculations with Spalart-Almaras turbulence closure model, run with the experimental boundary conditions, agree well with the test data, especially in terms of dependencies of the leakage loss magnitude on the relative movement between the blade and the casing. It is interesting that, contrary to the tendency in the leakage loss to decrease, the computed tip leakage mass flow rate increases with moving endwall. The computations show two distinct regions of high entropy creation rate near the blade tip. The first one is located close to the blade suction surface where the leakage flow leaves the clearance gap. The second one is located further from the suction surface and the entropy creation rate in this region decreases when the casing is in movement. This paper attempts to provide a qualitative analysis of the flow mechanisms involved in the entropy generation in the second regions. Finally Computations of a high loaded rotor show that the second region identified in the static cascade may also be present in rotating cascades.

INTRODUCTION

Storer and Cumpsty [1] & [2] investigated the behavior of the tip leakage flow in a linear cascade. They demonstrated that the static pressure field near the end of the blade controls the chordwise distribution of the flow across the clearance gap. With the help of numerical simulations, they established that the entropy generation takes place in the vicinity of the blade suction surface where the interaction of the tip leakage flow with the main stream forms a high dissipation rate shear layer. They developed a model to predict the leakage loss, in terms of the chordwise average angle of the leakage flow direction to the blade suction surface, which showed good agreement with measurements. Denton [3] also proposed a model for predicting the entropy creation in terms of the blade pressure distribution. He also considered that most of the entropy was created near the blade suction surface and that the understanding of how the leakage flow rolls into a vortex was not necessary to correctly predict the leakage loss. Shao et Al. [4] used the model developed by Denton to investigate the influence of the blade loading and tip clearance distribution on the leakage loss. Further details about this model will be discussed later as a basic for the investigation of the entropy generation mechanisms. The Authors cited above did not take into account the relative motion of the endwall. Doukelis at al. [5] ran experiments in a high speed annular cascade with static and

moving hub. The performance of the cascade was improved by the relative motion of the hub. The explanation given for the performance improvement was a change in the inlet flow conditions. Through numerical simulations Inoue et al. [6] as well as William et al. [7] observed that despite an increase in the leakage flow and leakage vortex intensity the endwall motion decreased the loss in the tip region of a rotor blade. Several authors have thus observed that the relative endwall motion has a positive effect on the performance of a compressor blade row but no consensus has been found to explain this effect. The purpose of the present study is first to verify the latter effect and second, to clarify the mechanisms by which it modifies the leakage flow and loss.

NOMENCLATURE

ψ	Flow coefficient
V	Velocity
ξ	Pressure loss coefficient
P	Total pressure
p	Static pressure
ρ	Density
U	Tip leakage velocity
m	Clearance mass flow
M	Blade passage mass flow
TCL	Tip clearance gap height
L	Chord length
Cd	Clearance gap discharge coefficient
s	Entropy
Φ	Viscous dissipation function

Subscripts:

x	Axial
b	Belt
in	Inlet
cl	clearance
p	pressure side
s	suction side
inv.	Inviscid

EXPERIMENTAL APPARATUS

Experimental results were obtained at the linear cascade test facility of Iwate University described by Kato at al in reference 8. Figure 1 shows a schematic of the whole apparatus. It is composed of a blower equipped with a valve that allows regulating the inlet air mass flow. The air flows through a diffuser and a nozzle before entering the cascade which is composed of seven blades with a constant cross section from hub to tip. Table 1 lists some parameters of the cascade. The airfoil cross section is representative of a typical rotor blade used in the rear stages of high loaded axial compressors. The cascade exit pressure is adjusted by two punched metal panels. A belt moved by an electric motor and a system of pulley simulates the relative motion of the casing. The belt is mounted on a frame placed below the cascade. The clearance gap between the belt and the blade tip can be adjusted by changing the blade height. Figure 2 shows the measurement locations. Pressure and flow angle are measured by a five holes Pitot-probe coupled with a traverse apparatus at plane S0, located 30% chord upstream of the blades leading edge and plane S1, located 16% chord downstream of the blades trailing edge. The measurements planes extend from 6% to 96% blade height from the hub surface in the span-wise direction and two blade pitches in the pitch-wise direction.

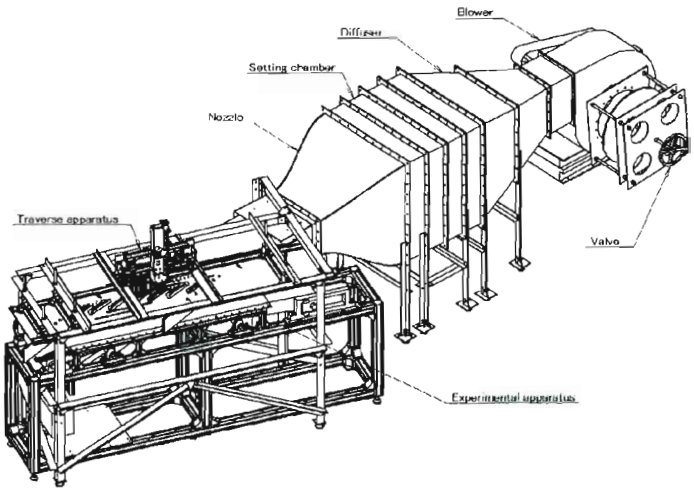

Figure 1 Schematic of the test Facility

Table1 Blade geometrical characteristics

Chord length (m)	0.237
Solidity	1.35
Blade height (m)	0.168
Stagger (deg.)	58.43
Camber (deg.)	30.3
Re Number	$1x10^5$

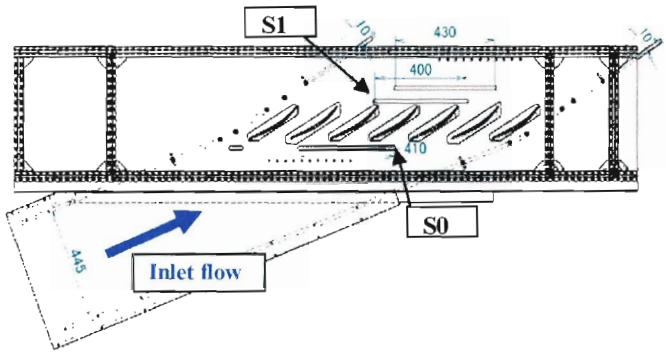

Figure 2 Measurement section

CONFIGURATIONS STUDIED AND TEST RESULTS

Measurements were realized at 0%, 2% and 4% clearance to blade height. At 2% and 4%, measurements were carried out with both static and moving endwall. The endwall speed was chosen such as to obtain a flow coefficient of 0.38. The flow coefficient is defined by equation 1 where V_x is the axial velocity at the cascade inlet and V_b is the belt velocity, equal to 6 m/s. This choice allows the ratio of the leakage velocity to the endwall velocity being of the same order as a rear stage rotor blade operating at design condition. It will be shown later that the leakage flow velocity relative to the endwall velocity plays an important role in the loss generation.

$$\phi = \frac{V_x}{V_b} \tag{1}$$

Figure 4a and 4b shows the incidence contours at 2% clearance respectively for static and moving endwall. Inlet conditions are quite uniform from blade to blade in the pitch-wise direction of the measurement plane. The motion of the endwall only slightly influences the inlet flow angle and it is considered that this change, which is less than 0.5 degree, does not affect the two-dimensional loss of the cascade which still operates near design point. The loss contours shown in figures 5a and 5b respectively for static and moving endwall were calculated using equation 2 where P_{in} and V_{in} are the inlet average total pressure and velocity measured at plane S0, and P(y,z) is the local total pressure at coordinates y,z lying on plane S1. They clearly show a reduction in the tip loss associate with an increase in the hub loss with the endwall motion. The reduction in the tip blockage with moving wall leads to a higher diffusion in the hub region affecting the secondary flow. Despite the increase in the hub loss the wall motion reduces the total pressure loss of the cascade by about 13%.

$$\zeta(y,z) = \frac{[P_{in} - P(y,z)]}{0.5\rho V_{in}^{\ 2}} \tag{2}$$

The experimental results were used to validate the numerical analysis described below, which in turn provided a detailed description of the leakage flow. Simulations at 2% clearance with static and moving endwall were compared with the test data.

NUMERICAL SIMULATIONS

Numerical simulations were run using UPACS, a CFD codes developed by JAXA (Japan Aerospace Exploration Agency). The Spallart-Almaras model is used to simulate the turbulent flow. Total pressure and flow angle span-wise distribution measured at plane S0 were used as inlet boundary conditions for the calculations. The mesh is shown in figure 6. It is composed of an O-mesh surrounding the blade section that assure no skewed grid near the blade surface, and an H-mesh near the inlet and exit boundaries. Figure 7a and 7b shows the loss contours computed at plane S1 respectively for moving and static endwall; with moving endwall, the reduction in tip leakage loss along with the increase in hub loss are well captured by the CFD. However, the computed hub corner separation and mid-span loss are overestimated for both static and moving endwall. The turbulent model in use for the calculations is a full turbulent one and thus unable to capture any turbulent transition on the blade surface. At low Reynolds number, as it is the case in the present calculation, the accuracy of the profile loss prediction is altered. The measured and computed span-wise loss profiles at the cascade exit are shown in figure 8. The horizontal axis represents the loss averaged over the measurement plane width (pitch direction), and the vertical axis represents the blade span from hub to tip.

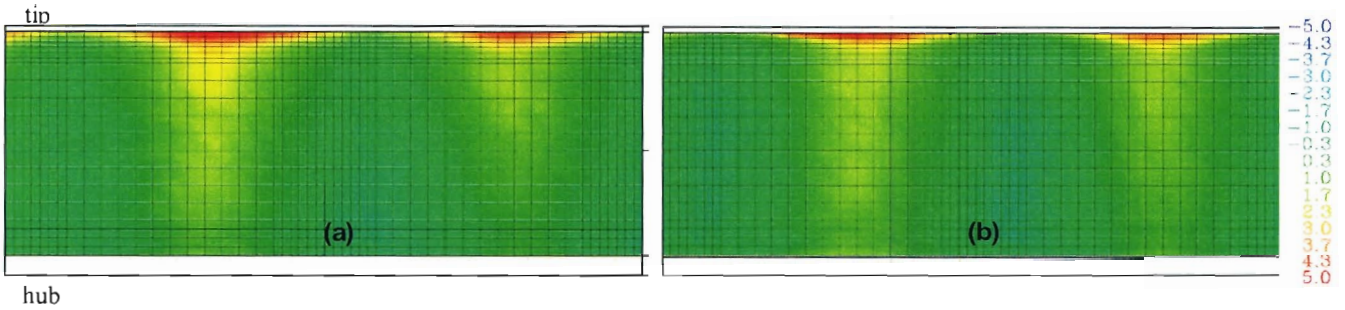

Figure 4 Test results: Incidence contours at Plane S0, at clearance 2%. **(a)** Static endwall, **(b)** Moving endwall

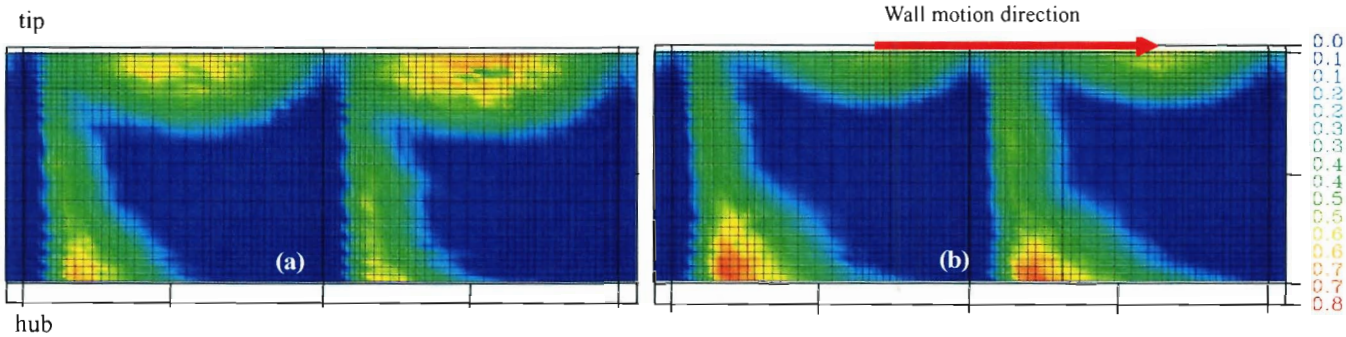

Figure 5 Test results: Total pressure loss contours at Plane S1, at clearance 2% **(c)** Static endwall, **(d)** Moving endwall,

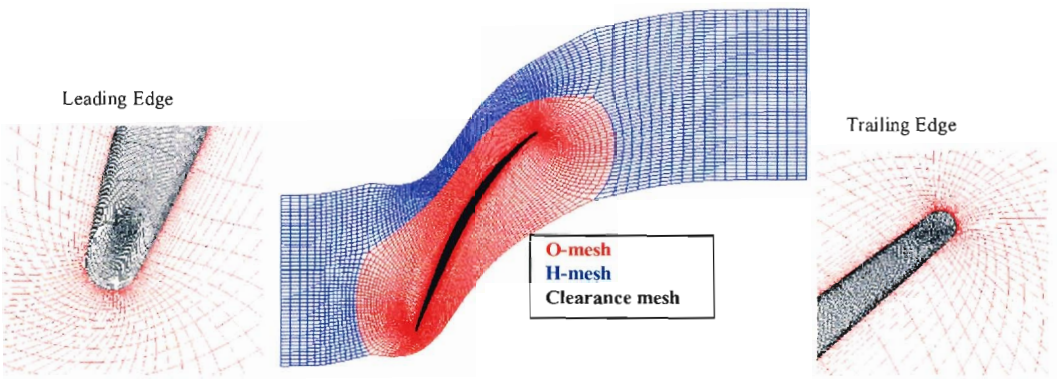

Figure 6 Calculation mesh

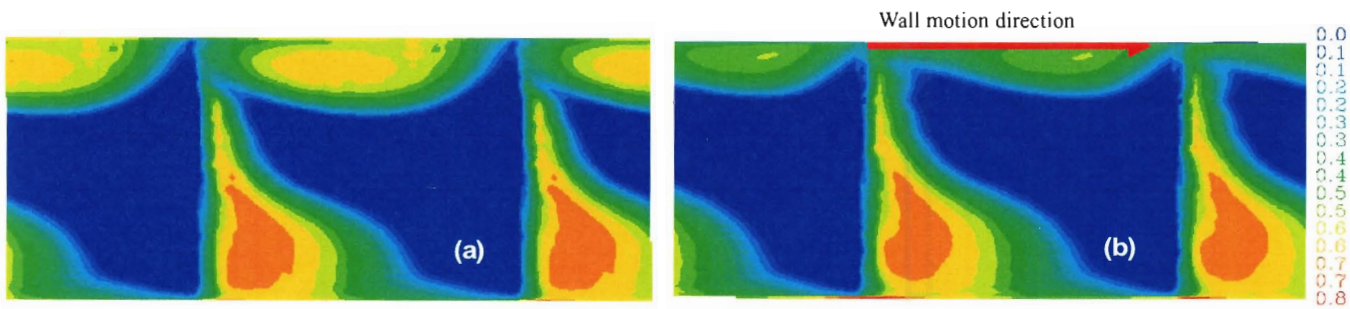

Figure 7 CFD results: Total pressure loss contours at Plane S1. **(a)** Clearance 2% static endwall, **(b)** Clearance 2% moving endwall

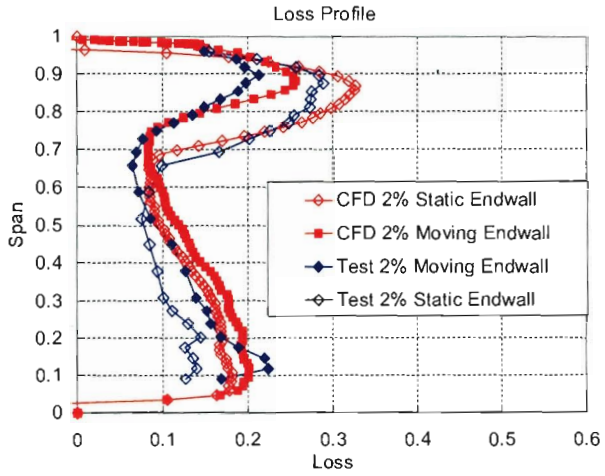

Figure 8.Loss profile at 2% clearance

The computed tip leakage loss level and affected span agree well with the test data for both static and moving endwall. CFD seems to correctly simulate the effect of the endwall movement on the tip leakage loss. Although discrepancies between tests and simulations are observed at hub and mid-span, and since the study focus on the leakage flow mechanisms, simulation results are considered sufficiently accurate for further investigations of the leakage flow and loss generation mechanisms.

DISCUSSION

The tip leakage mixing process

The model proposed by Denton in reference 3 predicts the entropy creation in terms of the leakage flow passing over the blade tip and the difference between the stream-wise velocity components of the leakage flow and the mainstream. It is assumed and that the stream-wise component of the leakage flow does not change through the clearance gap i.e. if the blade is sufficiently thin as it is the case for compressor blades, the leakage mass flow leaves the clearance gap with a stream-wise velocity equal to the local pressure surface velocity V_p and reaches the main stream which velocity is equal to the suction surface velocity V_s. The velocity vector difference between the two streams enhances the formation of a shear layer near the suction surface where the energy dissipation occurs. The total entropy created in the shear layer is estimated by integrating equation 3 over the chord length, where 'dm' is the leakage mass flow over a small portion of chord.

$$T\Delta S = V_s \times (V_s - V_p) \times \frac{dm}{M} \tag{3}$$

Influence of the endwall movement on the leakage mass flow.

Figure 9 shows the chord-wise distribution of the tip leakage velocity component normal to the blade suction surface computed from the CFD results. The leakage flow velocity increases with the endwall movement. Two explanations can be given for this increase; the first one is a change in the blade surface pressure as shown in figure 10. With moving endwall the blade loading is slightly increased along with the leakage velocity. The second explanation involves the viscous effects inside the clearance gap which were described by Nikolos et al. in reference 9. Viscous effects near a casing in movement relative to the blade tip help driving the leakage flow from pressure to suction surface, whereas near a static casing they tend to block it. Also shown in figure 9 is the leakage velocity U_{inv} calculated with equation 4 (Bernoulli equation) by using the computed blade pressure distribution near the tip (figure 9). U_{inv} represents the leakage velocity at the exit of the clearance gap if no viscous effect were acting on the leakage flow.

$$U_{inv} = \sqrt{\frac{2(p_p - p_s)}{\rho}} \tag{4}$$

As the simulation intrinsically takes into account the viscous effects, the leakage flow velocity directly computed from the CFD results is lower than the one calculated with Bernoulli equation. The leakage mass flow 'dm' over a small portion of chord appearing in equation 3 is calculated using equation 5, where U is the local leakage flow velocity at a given location along the blade chord and averaged over the clearance gap height.

$$dm = \rho_{cl} U \times TCL \times dL \tag{5}$$

By integrating equation 5 over the blade chord one can obtain the total tip leakage mass flow. Table 2 shows the leakage mass flow in percentage of the blade passage mass flow computed from the CFD results and calculated with Bernoulli equation. The 10% increase in leakage mass flow from static to moving endwall, computed from the CFD results, is due to the change in the airfoil loading as well as viscous effects near the casing; whereas the increase in leakage mass flow calculated with Bernoulli equation is only due to the change in blade loading. The clearance gap discharge coefficient 'Cd', introduced in references 2 and 3, and shown in the fourth column of table 2 represents the ratio of the actual leakage mass flow to the ideal one. The actual leakage mass flow being estimated as the leakage mass flow computed from the CFD results and the ideal leakage mass flow being calculated with Bernoulli equation. With moving endwall, the estimated discharge coefficient is 5% higher than with static endwall, which means that half of the increase in leakage mass flow with moving endwall is due to viscous effects, the other half being caused by the change in blade loading.

In the leakage loss model described above, the leakage mass flow calculated with Bernoulli equation is usually adjusted by the discharge coefficient in order to take into account the viscous effects through the tip clearance gap.

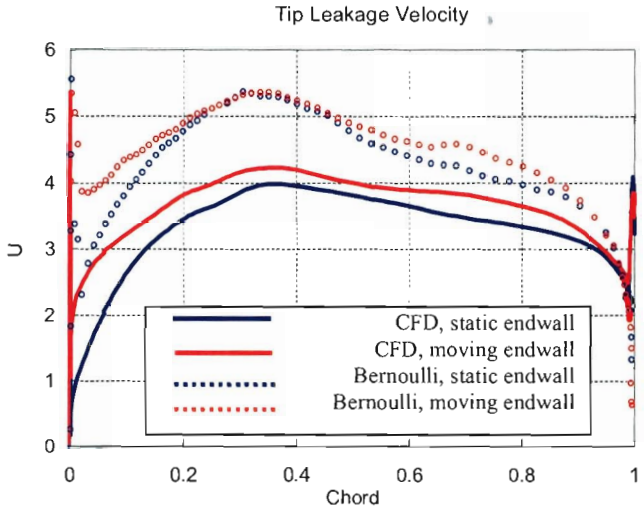

Figure 9 Leakage flow velocity component normal to the blade suction surface.

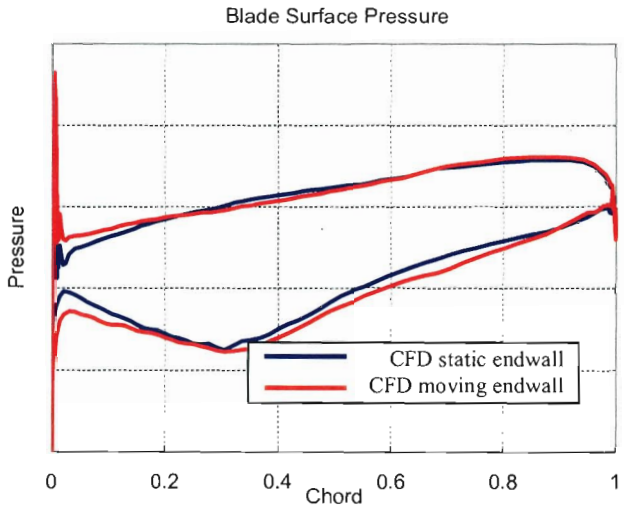

Figure 10 Blade surface pressure near tip

Table2 Leakage Mass flow

Leakage Mass Flow (%passage mass flow)	CFD (viscous)	Bernoulli (inviscid)	Cd
Static Endwall	3.55	4.56	0.78
Moving Endwall	3.92	4.79	0.82

Influence of the casing movement on the entropy generation

Calculation results obtained with the model developed by Denton are compared with the test data in figure 11. Measured and predicted loss increase almost linearly with the clearance gap height. The computed blade surface pressure distributions shown in figure 10 were used as input for the model as well as the estimated discharge coefficient shown in table 2. Predicted losses were added to the measured loss at 0% clearance to allow the comparison with the test data.

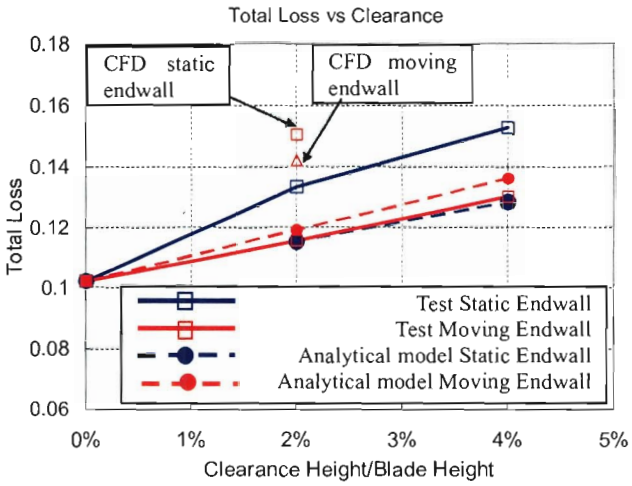

Figure 11 comparisons between test, simulation and analytical model

The increase in leakage mass flow leads the model to predict greater losses with moving endwall, whereas test results show the opposite trend. The model is quite accurate for moving endwall but underestimates the loss for static endwall. In order to explain this discrepancy, the entropy sources were identified by computing the entropy creation rate (hereafter called dissipation), defined by equation 6, from the numerical results.

$$\rho U.\nabla s = \frac{\Phi}{T} + \frac{k}{T}\nabla^2 T \tag{6}$$

As mentioned in reference 2, for low Mach number flow without heat transfer, the only source of entropy is the viscous dissipation Φ defined by equation 7.

$$\Phi = -\left(u\frac{\partial P_0}{\partial x} + v\frac{\partial P_0}{\partial y}\right) \tag{7}$$

Figures 10a and 10b show the dissipation contours on a plane perpendicular to the blade stacking axis at a vertical location corresponding to the blade tip respectively for static and moving endwall. The shear layer formed near the blade suction surface and denoted by 'region 1' is clearly visible at both static and moving endwall conditions. With moving endwall the dissipation is slightly more intense than with static

endwall due the higher leakage mass flow rate. Figures 11a and 11b show the dissipation contours at a vertical location of 70% clearance gap height from the blade tip. With static endwall, a high dissipation region denoted by 'region 2' is formed away from the suction surface. With moving endwall the same region is present but located further from the suction surface with a much less intense dissipation than with static endwall. Despite the shear layer adjacent to the suction surface (region 1) dissipates more energy with moving endwall; the total loss and thus entropy creation is greater with static endwall due to the presence of region 2, in which the entropy created is not predicted by the model described above. Figure 12 shows the dissipation contours in planes perpendicular to the suction surface in order to illustrate the depth of the region 2.

Entropy Generation Mecchanisms

In region 1, the dissipation intensity increases from static to moving endwall but the mechanism by which the entropy is created is not modified. This is illustrated in figures 13a and 13b, which shows the streamlines crossing region 1. For both moving and static endwall, the streamlines that mix into the shear layer come from the clearance gap and from the vicinity of the blade suction surface.

Figure 14a illustrates the mechanisms involved in the entropy creation in region 2 for static endwall. The interaction between streamlines from the main stream, departing away from the blade suction surface and leakage streamlines leaving the clearance gap very near the endwall are at the origin of the dissipation. The pressure gradient in the blade passage forces the main stream to migrate across the blade passage toward the suction surface and to reach the leakage flow. As the two streams have different velocities and directions, their mixing enhances high dissipation. When existing, the relative movement of the casing counteracts the blade passage pressure gradient preventing the main stream migration and its interaction with the leakage flow. Although the dissipation in region 2 is much less intense, the region is still visible when the endwall is in motion.

Figure 14b shows the streamlines crossing region 2 at moving endwall condition, leakage streamlines exiting the clearance gap at different locations are involved in the formation of region 2. The location of region 2 corresponds to a chord location where the leakage velocity (shown in figure 9) reaches its maximum. The leakage flow exiting the clearance gap upstream the leakage flow peak velocity is driven in the endwall direction soon after leaving the gap, whereas at the peak velocity location, the leakage flow possesses enough kinetic energy not to be driven by the moving endwall, it follows a straight trajectory until it reach the leakage flow coming from upstream. The difference in velocity and direction of the streams involved in the mixing is much lower than at static endwall conditions, which explains the less intense dissipation.

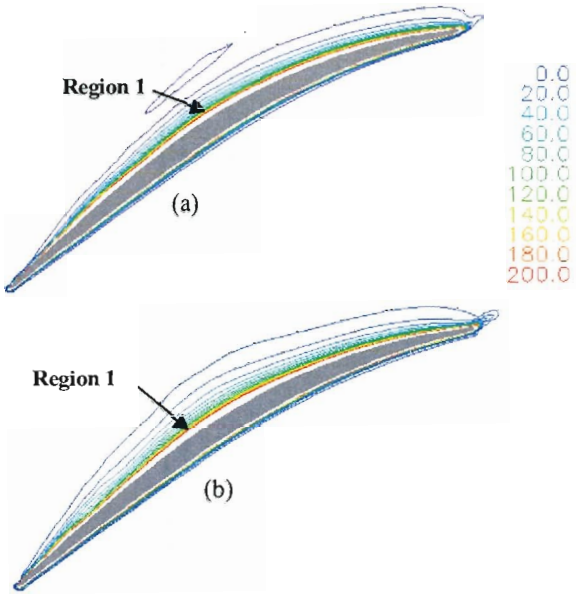

Figure 10 dissipation contours at blade tip, **(a)** Static endwall, **(b)** Moving endwall

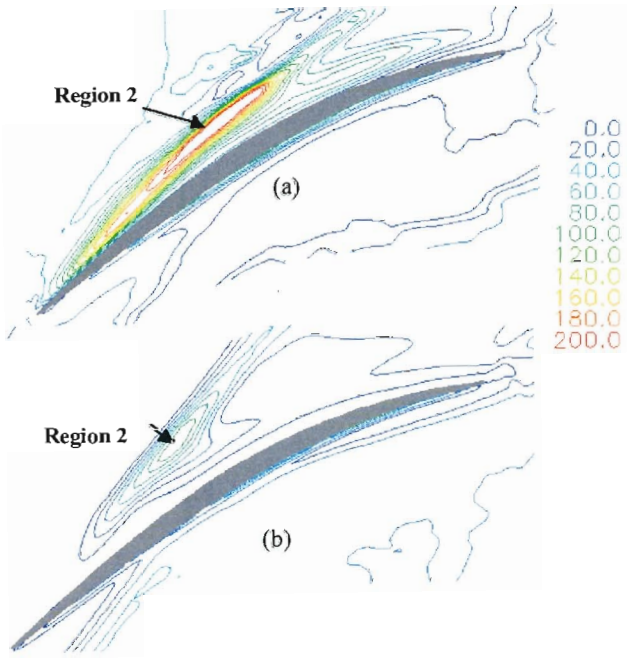

Figure 11 dissipation contours at 70% clearance gap height from the blade tip, **(a)** Static endwall, **(b)** Moving endwall

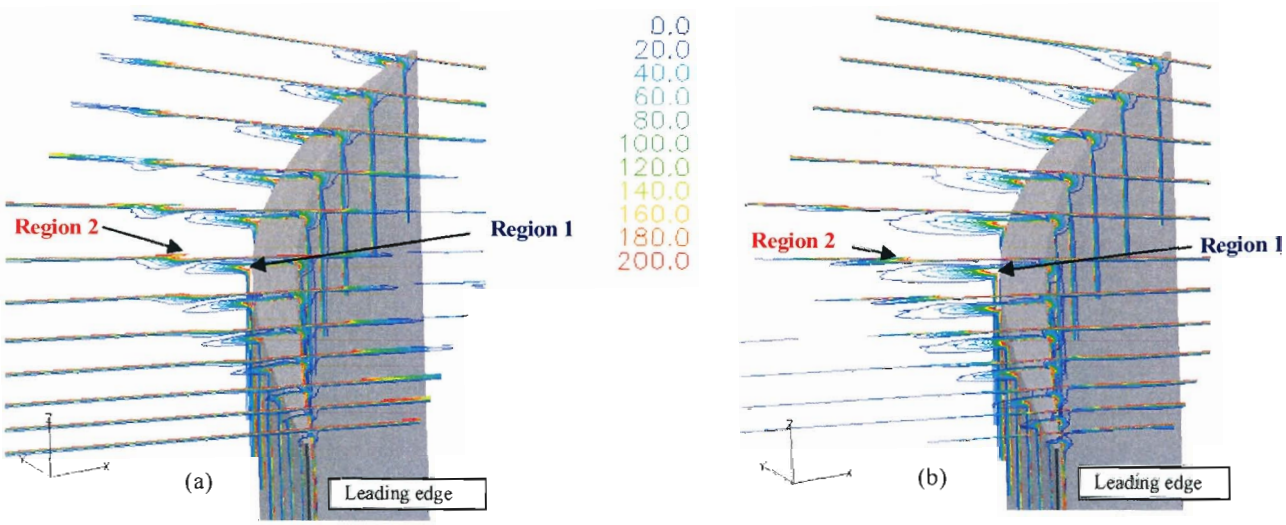

Figure 12 Dissipation contours at different plane perpendicular to the blade suction surface, **(a)** Static endwall, **(b)** Moving endwall

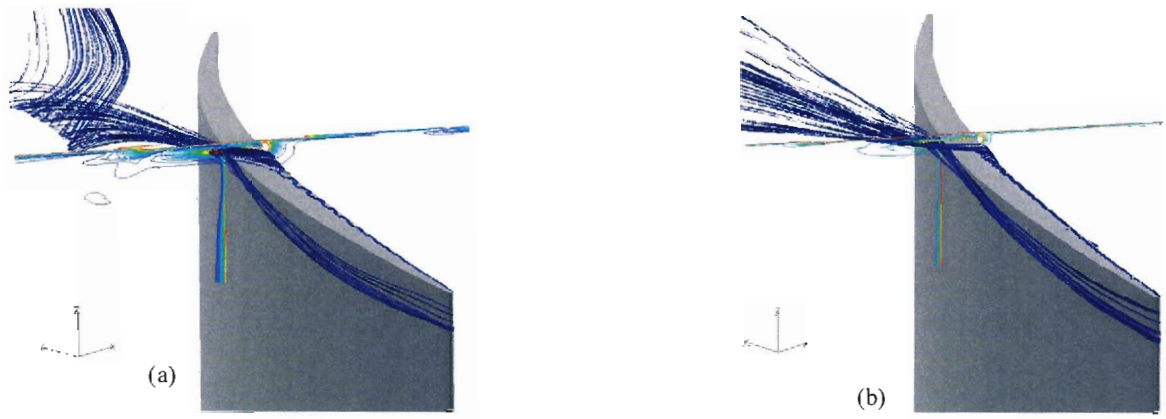

Figure 13 Streamlines crossing region 1, **(a)** Static endwall, **(b)** Moving endwall

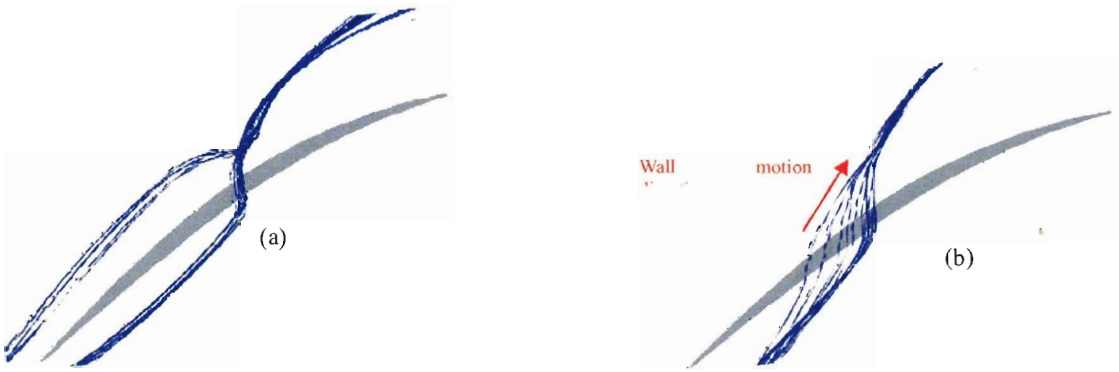

Figure 14 Streamlines crossing region 2, **(a)** Static endwall, **(b)** Moving endwall

Leakage loss Mechanisms in rotating cascade

In rotating cascades, the casing is in motion relative to the blade tip; according to the previous results obtained with the static cascade, this would limit or suppress the entropy creation away from the blade surface (region 2). However the investigation of the leakage flow of a relatively high loaded rotor through numerical simulations shows that this assumption is not always true. Figure 15 shows the dissipation contours resulting from the simulation at 70% tip clearance gap height from the blade tip at design point and near stall. A region similar to region 2 is observed at both conditions but its length at near stall is more than twice its length at design points. As well as for the static cascade with moving endwall, the chord location where the dissipation rate is at its maximum corresponds to the chord location of the peak leakage flow velocity which chord-wise distribution is shown in figure 16. Near stall the peak leakage velocity is greater than at design point and its peak location is shifted toward the leading edge along with the peak dissipation.

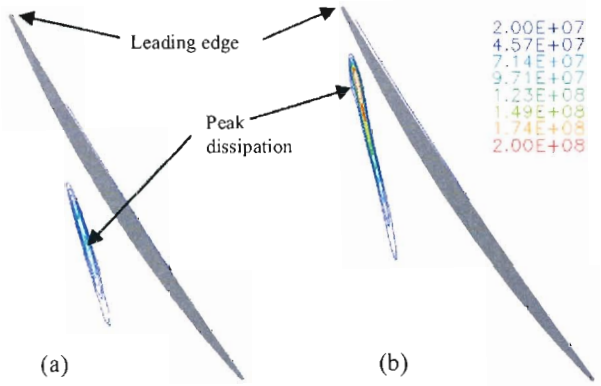

Figure 15 Dissipation contours at 70% clearance height from the blade tip **(a)** At design point, **(b)** Near stall

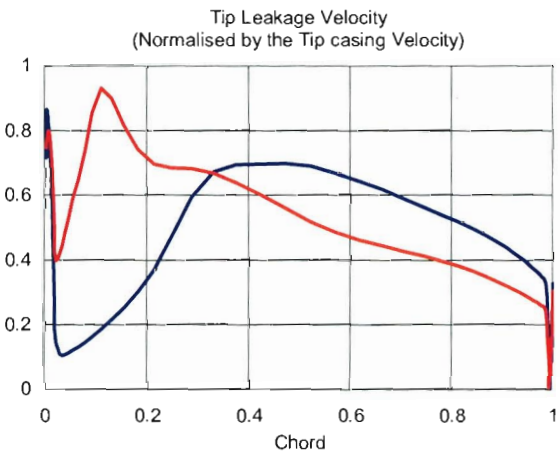

Figure 16 Leakage flow velocity component perpendicular to the blade suction surface normalized by the tip casing velocity

CONCLUSION

Tests carried out in a static cascade facility equipped with moving endwall show that the tip leakage loss decreases with the endwall motion. CFD simulations of the cascade run in the test conditions also show a decrease in the leakage loss with the endwall motion, whereas the computed leakage mass flow crossing the clearance gap tends to increase. The analysis of the numerical results shows two distinct regions of high entropy generation rate; a first one located near the blade suction surface and a second one located further from it. In the first region the entropy creation is intensified when the endwall is in motion, whereas in the second one it is largely decreased. At static endwall condition, the entropy generated in the second region is due to the interation of the leakage flow with the passage flow away from the suction surface. At moving endwall condition, the decrease in entropy creation rate in this region comes from the fact that, in the very vicinity of the casing, the endwall motion tends to drive the passage flow and the clearance flow in the same direction preventing an intense mixing between the two streams. However, the region itself does not completely disappear and is still visible at an axial location where the leakage flow velocity is high compare to the endwall velocity; at such location, the leakage flow leaving the clearance gap possesses sufficiently high kinetic energy not to be driven by the casing motion, which lead to its mixing with the upstream leakage flow.

Simulations of a rotating cascade show that a high dissipation region away from the suction surface, similar to the one observed for the static cascade, is visible. The intensity of the dissipation in this region increases from design point to near stall. Future prospects are a quantitative evaluation of the impact of the loss generated in region 2 on the overall performance of rotating cascades, and the development of a loss model that takes into account the leakage flow velocity relative to the endwall velocity.

ACKNOWLEDGMENTS

The authors would like to thank the students of Iwate University for conducting the cascade tests and test data analysis.

REFERENCES

[1] Storer J. A., Cumpsty N. A., 1990, "Tip Leakage Flow in Axial Compressors", ASME paper 90-GT-127.

[2] Storer J. A., Cumpsty N. A., 1993, "An Approximate Analysis and Prediction Method for Tip Clearance Loss in Axial Compressor", ASME paper 93-GT-140.

[3] Denton J. D. 1993, "Loss Mechanisms in Turbomachines", ASME Journal of Tubomachinery, vol. 115, No. 4, pp621-657.

[4] Shao W., Ji L. 2007, "Basic Analysis of the Tip Leakage Mixing Loss", ASME paper GT2007-27616.

[5] Doukelis A., Mathioudakis K., Papailiou K., 1998, "The Effect of Tip Clearance Gap Size and Wall Rotation on the Performance of a High-Speed Annular Compressor Cascade", ASME paper 98-GT-38.

[6] Inoue M., Furukawa M., Saiki K., Yamada K., 1998 "Physical Explanations of Tip Leakage Flow Field in an Axial Compressor", ASME paper 98-GT-91.
[7] William R., Gregory-Smith D., He L., 2006 "A Study of Large Tip Clearance Flows in an Axial Compressor Blade Row", ASME paper GT2006-90463.
[8] Kato H., Taniguchi H., Funazaki K., Kato D, Pallot G., 2010, "Experimental and Numerical Investigation on Compressor Cascade Flows with Tip Clearance at a Low Reynolds Number Condition", 3rd Asian Joint Workshop on Thermophysics and Fluid Science paper JP-41.
[9] Nikolos I. K., Douvikas, D. J., Papaliou K. D., 1995, "Theoritical Modelling of Relative Wall Motion Effects in tip Leakage Flow", ASME paper 95-GT-88.